

Concept Paper

Two-Level Electron Excitations and Distinctive Physical Properties of Al-Cu-Fe Quasicrystals

Alexandre Prekul * and Natalya Shchegolikhina

Institute of Metal Physics, Ural Branch of the Russian Academy of Sciences, 620990 Ekaterinburg, Russia; shchegol@imp.uran.ru

* Correspondence: prekul@imp.uran.ru; Tel.: +7-982-6058425

Academic Editor: Enrique Maciá Barber

Received: 1 July 2016; Accepted: 12 September 2016; Published: 19 September 2016

Abstract: This article is not a review in the conventional sense. Rather, it is a monographic study of the implications of detection in Al-Cu-Fe quasicrystals of the electronic heat capacity contributions associated with the two-level electron excitations. Our aim was to reveal correlations between these contributions, on the one hand, and specific features of electron transport, magnetic susceptibility, Hall-effect, tunnelling and optical spectra, on the other hand. It is shown that the full range of these features can be understood in the framework of the unified conceptual scheme based on two-level electron excitations.

Keywords: quasicrystals; electronic structure; two-level electron excitations

1. Introduction

Quasicrystals in general and icosahedral (i-) phases in particular have attracted the interest of scientists, not only because of their exotic lattice structure. A question that arises from the very beginning is why nature should prefer quasiperiodic to periodic order. The lattice structure of these phases is based on an icosahedron, i.e., a polyhedron that has fivefold symmetry and cannot serve as a unit cell of a periodic crystal. It is clear that minimization of the internal energy cannot be achieved without a decrease in the kinetic energy of free charge carriers. Now it is well known that the formation of icosahedral phases does lead to a significant reduction in the metallic properties of initial metals.

Due to this reduction, the icosahedral phases differ from conventional metals, both quantitatively and qualitatively. The main quantitative difference lies in the fact that these phases have an anomalously low ($\sim 10^{19-20} \text{ cm}^{-3}$) concentration of conduction carriers in the low temperature limit; i.e., the average valence (electrons/atom) in the alloy at low temperatures is $e/a \sim 10^{-3}$. As a consequence, the icosahedral phases have a low, but finite ($\sim 100 \Omega^{-1} \cdot \text{cm}^{-1}$), metal-like conductivity, as well as low values of the Pauli susceptibility and electronic heat capacity. These differences are reflected in the hypothesis of the pseudogap. According to photoelectron spectroscopy experiments, the pseudogap has a width of $\sim 1 \text{ eV}$ [1].

The main qualitative differences are associated with a significant variability of the number of charge carriers at finite temperatures. The concentration of thermally induced charge carriers (TICC) increases very rapidly with increasing temperature. At 1000 K, this concentration differs only slightly from the atomic density of the substance; i.e., the average valence in the alloy at high temperatures is $e/a \sim 1$. Consequently, an increase in the temperature leads to a very rapid increase in the electrical conductivity (negative TCR—temperature coefficient of resistivity) and to a very rapid enhancement in the paramagnetism. The amplitudes of these TICC-associated giant thermal effects are many times larger than those of the corresponding parameters of metal-like ground state carriers [2].

Since there are various aspects of the lattice structure, three scenarios of the reduction nature of the metallic properties in quasicrystals have been discussed in the literature. On the one hand, the

quasilattice has no long-range periodic order in the arrangement of atoms. In the general case, this means that quasicrystals are similar to disordered systems in which the Anderson localization can play a significant role [3]. On the other hand, quasicrystals have a long-range quasiperiodic order. Thus, they can be considered as a limiting case of the Hume-Rothery phases, where all wave vectors of the ideal quasilattice are vectors of reflection. At the Fermi level, ideally, there arises an energy gap, whereas in fact a pseudogap is formed. Finally, quasicrystals have an icosahedral short-range order. The reduction in the metallic properties can be associated with the confinement of initially valence electrons through the exchange coupling of electrons in the formation of chemically saturated (covalent) bonds [4–6].

A large number of experimental studies into the physical properties of stable icosahedral (i)-phases were performed soon after the discovery of these phases. The result of these studies was somehow paradoxical: no physical properties of i-phases assumed from their long-range quasiperiodic nature were identified [7]. Therefore, the long-range icosahedral order and the Hume–Rothery–Jones mechanism (a contact between the Brillouin zone boundaries and the Fermi surface) should be excluded from consideration, both based on the above mentioned paradox and on the fact that TICC-associated thermal effects are observed at temperatures higher than the melting temperature where the zone structure is destroyed [8,9]. The results of numerous experiments carried out to investigate the effect of quasilattice structural perfection on the electrical properties of quasicrystals (see [2] and references therein) also allow the structural disorder and the Anderson localization mechanism to be excluded from consideration. The reasoning is quite simple. The effect exerted by a structural disorder on the electrical conductivity of quasicrystals is opposite to that of the Anderson mechanism.

Insensitivity of TICC-associated effects to the aggregate state means also that the structure-forming factor of these effects is the short-range order in the spatial arrangement of atoms. Along with that, the following facts should be taken in consideration. Reference [10,11] provided a direct evidence of covalent bonds in the electron density distribution of AlMnSi and AlReSi icosahedral quasicrystalline 1/1 cubic approximants using a combination of the maximum-entropy method and the Rietveld method. In reference [12], the covalence in AlPdRe quasicrystals was experimentally confirmed from the atomic density and the quasilattice constant. Based on the data obtained, a conclusion was made that localization via exchange pairing is a dominant factor of the formation of the electronic structure of phases with the icosahedral short-range order and that pseudogap is a consequence of such localization.

Thus, among the above scenarios, the localization through the exchange coupling, which was justly called neither recurrent [5] nor chemical [6], but the Heitler-London (HL) localization by the authors of the first quantum mechanical theory of covalent binding [13], is considered to be the most possible scenario. Accordingly, the distinctive properties of i-phases should be associated with spatially localized electron excitations.

2. Features of the Electronic Specific Heat Capacity

Calorimetry has been traditionally considered an effective tool that provides information on the mechanisms of energy absorption by elementary electronic and lattice excitations. Therefore, calorimetric investigations were performed for a number of quasicrystalline compounds with different chemical compositions and structural qualities in various temperature ranges from ultralow temperatures to melting points [14–18]. Despite a large variety of objects, all these investigations share a common trait. It has been assumed that the electronic component of the specific heat of quasicrystals over the entire range of temperatures is determined by the contribution γT linear in the temperature, where γ is the Sommerfeld coefficient. As is known, this contribution is rather small. For typical metals at a charge carrier concentration of $\sim 10^{23} \text{ cm}^{-3}$ and room temperature, this contribution is no more than 0.5% of the lattice specific heat [19]. For quasicrystals, the corresponding contribution is even smaller and does not exceed 0.1%. This contribution was ignored, and the entire experimentally measured specific heat was considered to constitute the lattice specific heat.

Possibly, the approximation that the lattice plays a dominant role does not involve a large error but requires the justification for quasicrystals. The point is that the Sommerfeld model describes metal systems with a constant number of charge carriers. According to indications of a finite residual resistance and a linear electronic contribution to the specific heat at low temperatures, the quasicrystals are metals; however, they do not belong to systems with a constant number of charge carriers. At moderate and high temperatures, the number of TICCs can be several tens of times larger than the number of conduction band electrons in the ground state ($T = 0$ K) of the system [2].

Earlier we conducted a study of the specific heat capacity of quasicrystals of the Al-Cu-Fe system, with icosahedral phase samples having the $\text{Al}_{63}\text{Cu}_{25}\text{Fe}_{12}$ and $\text{Al}_{62}\text{Cu}_{25.5}\text{Fe}_{12.5}$ nominal compositions. The purpose of these experiments was to verify whether the linear-in-temperature metal-like contribution γT is the sole contribution to the electronic heat capacity of quasicrystals, or TICCs are capable of making their own contribution.

It is obvious that, if the heat capacity of singular electronic excitations exists, it will manifest itself as the excess heat capacity with respect to the sum of the lattice heat capacity C_{lat} and the metal-like heat capacity of ground state conduction electrons $C_{\text{ml}} = \gamma T$, that is,

$$C_{\text{exc}} = C_{\text{total}} - C_{\text{lat}} - C_{\text{ml}} \quad (1)$$

At the first stage, the measurements of the heat capacity and thermal expansion coefficient, which is necessary to convert C_p into C_v , were performed in the temperature range from 1.5 to 400 K. It is a well-studied region, where a noticeable increase in the electrical conductivity (negative TCR) and an enhancement in the paramagnetism have been observed and where, consequently, a singular contribution can manifest itself. It was found that the inclusion of the lattice heat capacity C_{lat} within the approximation of the Debye model leads to a very strong dependence of the final result on the model assumptions. To avoid this difficulty, we assessed a contribution of the lattice heat capacity C_{lat} in the approximation of the empirical Gruneisen law, which implies a linear relation of the lattice heat capacity to the linear expansion coefficient. Details can be found in [20,21].

The result turned out to be remarkable in two respects. On the one hand, the excess heat capacity is a curve with a maximum at about 90 K (Figure 1), which is well approximated by the Schottky function in the simplest case of two level excitations. This is shown by a solid line in Figure 1. On the other hand, the excess heat capacity almost completely disappears at near room temperature, whereas the singular thermal effects in both the electrical conductivity and the paramagnetism continue to increase with increasing temperature up to 1000–1200 K [2].

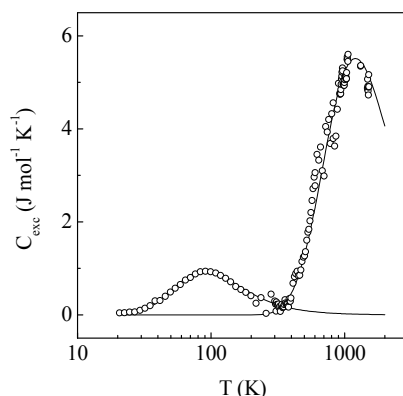


Figure 1. Temperature dependence of the excess electronic heat capacity of the $\text{Al}_{63}\text{Cu}_{25}\text{Fe}_{12}$ quasicrystalline alloy with respect to the Sommerfeld metallic contribution. Solid lines show the approximation of the curve by two Schottky contributions with excitation energies of 0.02 and 0.25 eV.

In order to clarify the situation, it was necessary to extend the calorimetric experiment to the high temperature range of 300–1000 K. We discovered that the excess heat capacity also appears and clearly manifests itself in the total heat capacity C_{total} at high temperatures significantly exceeding the Dulong-Petit limit. We determined the excess heat capacity in this temperature range with respect to this limit. The asymptotic approximation to this limit may be assessed using the Debye model, exactly which we chose to perform. Details can be found in [8,18].

As a result, we have observed a peculiar pattern. The high temperature excess heat capacity (see Figure 1) rather rapidly increases from 400 K, passes through an inflection point in the region of 750 K, and then continues to increase more slowly to the boundary of the experiment at 920 K. The experimentally revealed portion of the curve resembles the ascending branch of the Schottky thermal anomaly, but the further course of the curve remains unclear [22].

We performed further heat capacity measurements up to the region of 1650 K, which significantly exceeds the melting temperature of the substance (1280 K). The reason is that melting is preceded by solid phase structural transformations. The endothermic effects of these transformations in the temperature range of 1100–1280 K are so strong that the behaviour of the “base line” of the actual heat capacity of the substance within the boundaries of the solid state becomes undefined. The extension of the experiment further along the region of melts showed that the excess heat capacity of melts is a decreasing function of the temperature, i.e., the excess heat capacity curve has a maximum at about 1200 K and resembles the Schottky anomaly. The approximation by the Schottky function in the temperature of 400–1650 K is also shown by a solid line in Figure 1. It is quite satisfactory. Details of the experiment and the analysis results can be found in [8,9].

The results of all stages of the calorimetric experiment being generalized are shown in Figure 1. The resulting $C_{\text{TLE}}(T)$ curve is double peaked. It is unlikely that the heat capacity is a continuous function of the temperature. Rather, it consists of two functionally similar, but not interconnected parts; therefore their sum can be approximated by two contributions of the Schottky type [23] in the form of Equation (2) with excitation energies $\delta E_1 = 0.02$ eV and $\delta E_2 = 0.25$ eV, respectively.

$$C_{\text{TLE}} = N_1 k_B \frac{\left(\frac{\delta E_1}{k_B T}\right)^2 \exp\left(\frac{\delta E_1}{k_B T}\right)}{\left(1 + \exp\left(\frac{\delta E_1}{k_B T}\right)\right)^2} + N_2 k_B \frac{\left(\frac{\delta E_2}{k_B T}\right)^2 \exp\left(\frac{\delta E_2}{k_B T}\right)}{\left(1 + \exp\left(\frac{\delta E_2}{k_B T}\right)\right)^2} \quad (2)$$

According to the traditional treatment of the Schottky anomalies [23], the system under consideration has a few types of two-level excitations. They can be phason excitations, electron excitations or crystal field induced splitting of atom level excitations [14–17,22]. We noticed that the two-level excitations (TLE) density determined from the excess heat capacity is very close to the TICC density determined from the Hall-effect [20]. This is why we prefer electronic excitations to all other possibilities. We thereby postulated that the system under consideration has a few types of two-level electron traps—energetically and spatially well-localized states. The source of these traps may well be covalent binding mentioned above. The source of two-level excitations (TLE) may well be the splitting of the covalent binding state into “conjugated” (bonding/antibonding) levels.

In that case, the revealed features of the electron heat capacity turn out to be in good agreement with the HL-localization scenario.

3. A Two-Component Model of the Electronic Structure

In order to see whether the TLE concept provides a better understanding of the quasicrystals physics, we have considered a strongly structured density of states (DOS) model obtained by a formal superimposition of two sort of electronic spectra—continual and discrete. The continual spectrum is represented by the conduction band with a large pseudo-gap; the discrete one is represented by a set of extremely narrow pairwise conjugated levels—ground and excited—centred with respect to E_F . By suggesting that HL-localization (not the pseudogap) is the electron stabilizing factor of the quasilattice, we postulated also that the continual and discrete components are autonomic subsystems,

i.e., the thermally activated carriers do not get into the conduction band. They propagate on the excited levels of the traps by hopping or tunnelling.

It was surprising to discover that this naive model leads to highly interesting implications in understanding a number of experimental observations [24,25]. Let us briefly consider the main observations, which reveal the interconnection of the distinctive thermal effects with TLE density.

The heat capacity, as is known, reflects the rate of change in the internal energy of the system and, accordingly, the number of TLEs with variations in temperature. Therefore, during each stage of the investigation, we analysed the behaviour of the quantities that can be linearly related to the TLE concentration, namely, the increment in the internal energy of the system ΔU , the increment in the electrical conductivity $\Delta\sigma$, the increment in the magnetic parameter $\Delta(\chi T)$, and the increment in the inverse Hall effect $\Delta(1/R_H)$ in the specified temperature range [22]. With the attainment of the complete picture of the excess heat capacity and its approximation by two Schottky anomalies, there appeared a unique possibility to demonstrate this relation as a whole.

Figure 2 shows the temperature-induced components of the electrical conductivity, magnetic susceptibility and singular part of the internal energy $U_{TLE}(T)$. The latter dependence was obtained by the numerical integration of the experimental curve $C_{TLE}(T)$. Well-coordinated behaviour of all the curves is evident. On the other hand, the dependence $U(T)$ differs by obvious signs of alternating curvature, and the origin of this behaviour is clear enough. Since the singular heat capacity C_{TLE} , according to Equation (2), consists of two functionally similar parts, the temperature dependence of the number of TLEs also consists of two functionally similar contributions in the form:

$$N_{TLE} = \frac{N_1}{1 + \exp\left(\frac{\delta E_1}{k_B T}\right)} + \frac{N_2}{1 + \exp\left(\frac{\delta E_2}{k_B T}\right)} \quad (3)$$

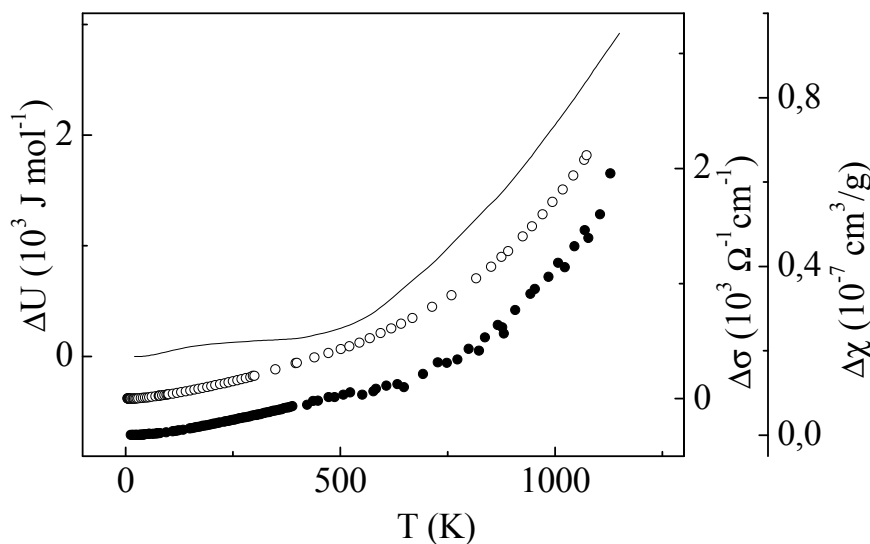


Figure 2. Curves of temperature-induced increments in the electrical conductivity $\Delta\sigma$ (open circles), paramagnetic susceptibility $\Delta\chi$ (closed circles), and internal energy ΔU (solid line) of the $Al_{63}Cu_{25}Fe_{12}$ icosahedral phase in the temperature range from 1.8 to 1000 K.

To make sure whether a change in the activation regimes takes place, we do not have to know each contribution separately. It is sufficient to construct the total curve $U(T)$ in the $\ln U(T)$ vs. T^{-1} coordinates, as shown in Figure 3a for the $Al_{63}Cu_{25}Fe_{12}$ icosahedral phase. A change in the activation regimes manifests itself in the fact that the curve has two linear portions. If the temperature dependent components of the electrical conductivity, the magnetic susceptibility, and the inverse Hall-effect,

where these contributions are very difficult or impossible to separate, are represented in the same coordinates, then, as seen in Figure 3b–d, there appear patterns that are identical to that in Figure 3a.

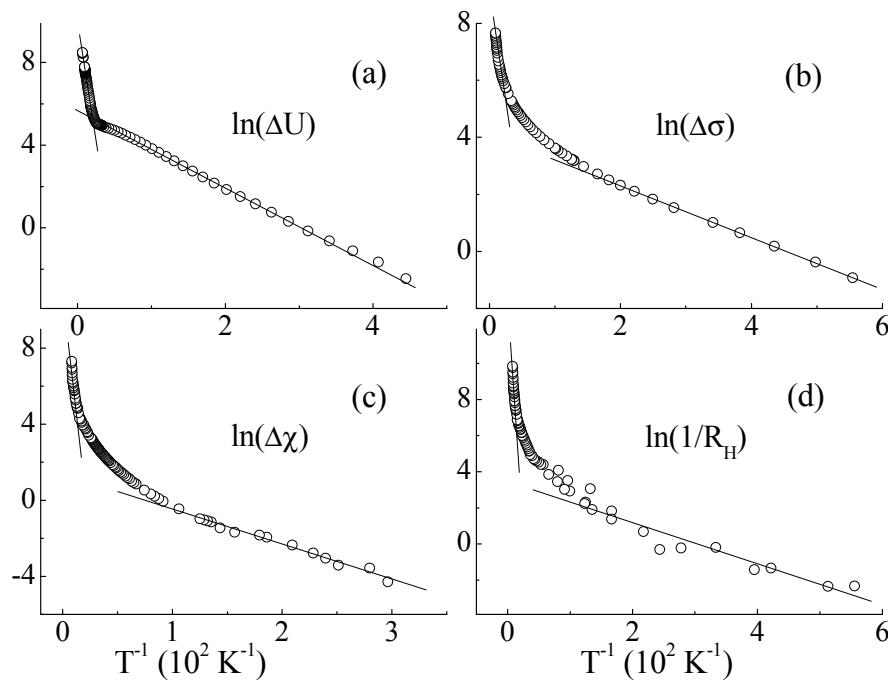


Figure 3. Change of regimes of thermal activation is a character feature of: two-level excitation density (a); conductivity (b); magnetic susceptibility (c); and inverse Hall effect (d) in the $\text{Al}_{63}\text{Cu}_{25}\text{Fe}_{12}$ phase.

The well-coordinated behaviour of all the curves on Figure 2 and the activation regime changes on Figure 3 mean a direct dependence of the thermally-induced giant effects on TLEs.

The singular heat capacity and singular paramagnetism are trivial implications of TLEs. The understanding of this phenomenon does not require new knowledge. It is sufficient to remember that the ground state of each trap is diamagnetic. The excited state of each trap is paramagnetic. The rest are determined by the population of the states according to Equation (2). A different situation occurs with the TLE conductivity. The case in point is the conduction over the excited states of the same type traps is carried out by hopping or tunnelling. We have not found a theoretical justification of such conductivity in the literature. From the experimental point of view, there is no difficulty in justifying this conductivity. If the conductivity of this type exists, it should manifest itself as an additive component to the conductivity of residual carriers, σ_{ml} . Qualitatively, this implication is confirmed by the empirical relationship known as Inverse Matthiessen Rule [26]. According to this rule, the electronic transport in quasicrystals is determined by additive contributions to the electrical conductivity, rather than to the electrical resistivity as in metals, i.e.:

$$\sigma(T) = \sigma_{\text{ml}} + \sigma_{\text{TICC}}. \quad (4)$$

Strange as it may seem, the most unusual postulate of our model that the continual and discrete components being autonomic subsystems coincide in energy is in agreement with experiment. Indeed, the threshold excitation energy obtained from the description of the low temperature part of the excess heat capacity is $\delta E_1 \sim 0.02 \text{ eV}$ and, as follows from the description of the high-temperature part of the excess heat capacity, it is $\delta E_2 \sim 0.25 \text{ eV}$. The pseudogap width, according to photoelectron spectroscopy, as was noted above, is equal to $\sim 1 \text{ eV}$. The Fermi energy of residual metal like carriers in the free electron approximation and at a charge carrier concentration of 10^{20} cm^{-3} is $E_F \sim 0.3 \text{ eV}$. It is easy to see that spatially localized states, if they exist, coincide in energy with the continuum of residual carriers.

In the framework of homogeneous localization models, such a coincidence is impossible [27]. It may mean that in quasicrystals, we are dealing with a special sort of inhomogeneous electronic system with a dual manifestation of inhomogeneity, namely, in the form of several generations of electron traps and in the form of the coexistence of extended and spatially localized states with the same energies. In any case, it means definitely that the conjugated levels of the traps should be separated by real gaps, not pseudogaps. To verify how realistic this implication we turned to the analysis of the spectral characteristics of quasicrystals.

4. Correlations between TLE Heat Capacity and Tunnelling Spectra

Icosahedral phases in aluminium alloys with transition metals have been actively studied in the last two decades by scanning tunnelling spectroscopy and point contact spectroscopy methods with various types of junctions—planar [28,29], point [30,31], and break [31,32]. It was shown that the dependences of the tunnel conductance ($G = dI/dV$) on the bias voltage (V) are strongly nonlinear characteristics exhibiting numerous features such as zero bias anomalies (ZBA), maxima, humps, and inflection points with a characteristic scale of several units to several hundred meV.

The fine structure of $G(V)$ curves is usually explained by the fact that it is the image of the fine structure of the electron density of states near the Fermi level. In other words, it is implicitly assumed that the tunnel current through a quasicrystal junction is due to quantum transitions between delocalized states on different sides of the barrier. In the one-electron approximation, a quite reasonable picture of the electron density of states of the icosahedral structure is obtained in the form of a comb of extremely narrow peaks separated by pseudogaps [28–32].

At the same time, another remarkable feature of tunnel experiments remains neglected. The fine structure of $G(V)$ curves in quasicrystals strongly depends on the effective area of a tunnel junction. In the case of a large area of the junction ($>10 \text{ nm}^2$), $G(V)$ curves have an “averaged” shape with a sign-alternating curvature, but smoothly increase with V . In the case of a small area of the junction ($<1 \text{ nm}^2$), $G(V)$ curves have a “local” oscillatory shape.

In view of the pronounced topographic aspect of tunnel spectra, the authors of [33–36] concluded that an additive scheme of the tunnel conductance is implemented in quasicrystals. A $G(V)$ curve consists as if of two independent components: the field-independent part G_0 , which is due to remaining delocalized conduction electrons, and the field-dependent part G_v , which is due to energetically and spatially well localized electrons:

$$G(V) = G_0 + G_v \quad (5)$$

It turns out that the fine structure is inherent only in the component G_v . It is obvious that, in view of the spatial localization of the features of G_v , extremely narrow peaks of the density of states should be separated by real gaps rather than by pseudogaps. Consequently, multiple ZBA would be expected in the spectrum. However, this is not the case in experiments. A single ZBA is always observed near $V = 0$. This specificity of real spectra was the first reason for doubt that the fine structure of $G(V)$ curves is the direct image of the electron density of states [36] and for the possibility of another mechanism.

A topographic similarity of electronics states from the excess specific heat and from the field dependent part of tunnel spectra stimulated us to seek correlations between these characteristics. We directly compared the local and averaged $G(V)$ curves obtained in the experiments with break junctions for i-phase of $\text{Al}_{64}\text{Cu}_{23}\text{Fe}_{13}$ in [32] and the $C_{\text{TLE}}(T)$ curve that we obtained for the i-phase of $\text{Al}_{62}\text{Cu}_{25}\text{Fe}_{12}$ and obtained the picture shown in Figure 4. All results in this figure are in situ, but all curves are represented in the same energy format. It is seen that the tunnel and thermal characteristics have visually similar maxima (they are indicated by arrows in Figure 4) at close energies.

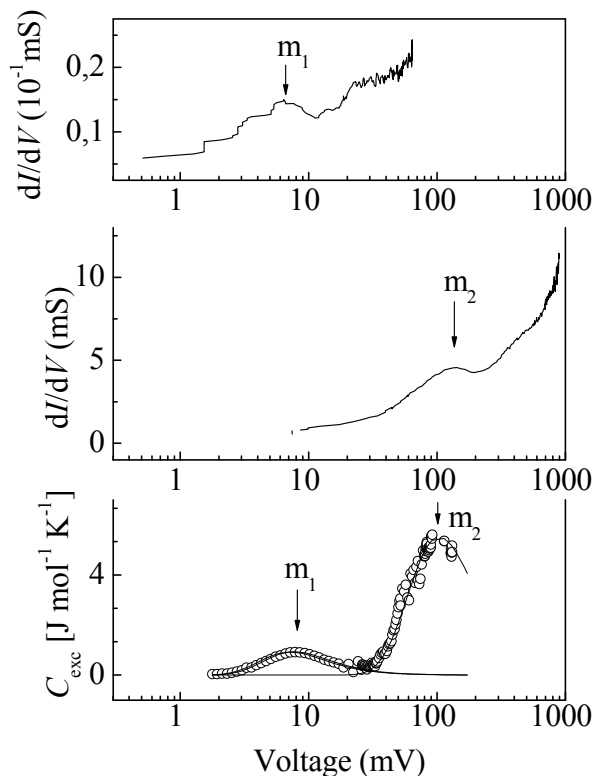


Figure 4. Visual comparison of the local and averaged tunnel spectra obtained in [32] and the excess electronic specific heat obtained in [25]. Arrows indicate features similar in shape and energy.

It was hypothesized that maxima of the tunnel conductance, as well as maxima of the excess specific heat, can be attributed to two-level excitations of electron traps. To this end, it should be assumed that quasicrystals contain charge carriers whose density depends on the electric field as the population of the upper level in the Schottky model depends on the temperature [23]:

$$N_{Vi} = N_{0i} / (1 + \exp(\delta E_i / V)) \tag{6}$$

Under the assumption that the mobility (μ_e) of these carriers slightly depends or does not depend on the field, it is easy to show that the conductance depends on V as:

$$G_i(V) = \mu_e dN_{Vi} / dV = \mu_e N_{0i} k_B \frac{(\delta V_i / V)^2 \exp(\delta V_i / V)}{(1 + \exp(\delta V_i / V))^2} \tag{7}$$

Because of the mathematical identity expressions, Equations (2) and (7), simple and clear understanding of the identity of heat and tunnel maxima is achieved.

This identity gives a key to the understanding of a microscopic mechanism of elementary electric terms. The thermal terms given by Equation (2) are by definition due to the internal thermal emission of electrons between conjugate levels of electron traps. Consequently, electrical terms given by Equation (7) are due to the internal field emission (Zener effect) [37] between the same levels. This fact is fundamentally changing the understanding of the fine structure of the tunnelling spectra.

By analogy with the excess specific heat, it is reasonable to expect that the field-dependent components G_v should generally be sums of numerous elementary terms given by Equation (7), differing in the splitting energy of conjugate levels of traps. Under this assumption, we analysed in detail the local and averaged $G_v(V)$ curves using Equation (7) as a trial function [38].

The thin solid line in Figure 5 is the local spectrum from [32] in direct energy coordinates. This curve clearly demonstrates the typical discussed features—ZBAs, pronounced maxima, and

pronounced humps. First, we approximate the maximum as the best-defined feature with the reference at the point of maximum. The result is shown by dash-dotted line 16. The description is not the best, but the reference to the maximum point gives the characteristic energy of two-level excitations $\delta E = 16$ meV, which is close to $\delta E = 19$ meV obtained from the specific heat [25]. The result is close to the expected one and is not unique. It is easy to see that dependence Equation (7) near $V = 0$ reproduces the ZBA feature of the tunnel spectrum.

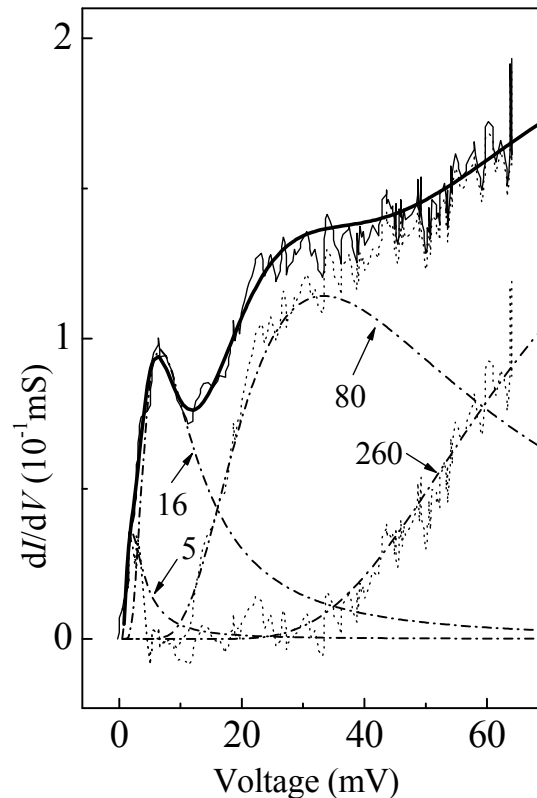


Figure 5. Deconvolution of the local $G(V)$ curve into elementary terms with the characteristic splitting energies of the levels $\delta E_i = 5, 16, 80,$ and 260 meV. The thin solid line is the experimental curve [32]. The dash-dotted lines are the elementary terms. The thick solid line is the sum of the terms. The dotted lines are residuals after subtraction of the terms.

We apply Equation (7) to approximate the difference between the local experimental curve and the calculated curve 16. This residual is shown in Figure 5 by the dotted line. It has a small maximum near 2 meV and a hump near 30 meV. The approximations of these two features by Equation (7) are shown by dash-dotted lines marked by the numerals 5 and 80 meaning δE_i corresponding to the best fit. The dotted line is a similar residual after the subtraction of lines 5, 16, and 80. This line has only one characteristic feature, ZBA, which is described by the dash-dotted line marked by the numeral 260. This residual is best approximated with the parameter $\delta E_i = 260$ meV, which almost coincides with the second characteristic energy of two-level excitations from the specific heat $\delta E_i = 250$ meV [25].

As is seen, the tunnel curve in the range $0 < V < 65$ meV is deconvoluted into four elementary terms with the energies 5, 16, 80, and 260 meV. The thick solid line in Figure 5 is the sum of these terms. The sum generally approximates the experimental data well. It is seen also that this sum leads to the hump features and to the fact that only a single ZBA with the smallest δE_i is visible. The remaining ZBAs become hidden.

Figure 6 shows the average spectrum from [32] in the energy range $0 < V < 850$ meV, which is significantly wider than the capabilities of a thermal experiment. The high-energy part of the curve exhibits two pronounced features: maximum and hump.

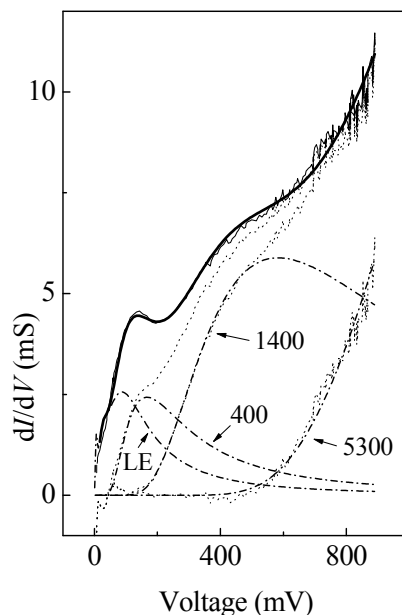


Figure 6. The averaged experimental $G(V)$ curve (thin solid line [32]) and its description (thick solid line) by the sum of the elementary terms with $\delta E_i = 5, 16, 80, 260, 400, 1400,$ and 5300 meV. The dash-dotted lines are the low-energy (LE) part of the spectrum and additional terms. The dotted lines are residuals after subtraction of the calculated curves.

The results of the analysis using Equation (7) are shown as dash-dotted lines in Figure 6. Additional elementary terms with the characteristic energies $\delta E_i = 400, 1400,$ and 5300 meV are detected. The procedure of their separation is similar to that described above. The only explanation that needs to be done relates to accounting the low-energy part of the spectrum in order to obtain a residual. The averaged curve in this part of the spectrum is strongly smoothed but is due seemingly to the same elementary terms as the above local curve. In view of this circumstance, to approximate the low-energy part of the spectrum at $V < 70$ meV, we used the entire set of “local” characteristic energies in the form of the LE contribution. This is the reason why the “high energy” residual shown by the dotted line in Figure 6 exhibits “dips” near $V = 0$. This does not affect the approximation of the high-energy residual of the averaged curve and this entire curve by the set of elementary terms (Equation (7)) with the characteristic energy gaps $\delta E_i = 5, 16, 80, 260, 400, 1400,$ and 5300 meV. The latter is shown by a thick solid line in Figure 6.

One may think that such a large number of gaps were used solely for the purpose of a qualitative fit. However, this is not exactly so.

5. Two-Level Excitations and Optical Spectra

It is well known that optical investigations, performed across a broad spectral range, are a powerful experimental tool for identifying the spectrum of excitations. We were able to identify a set of δE_i values as the real gaps. If so, a distinctive feature of the behaviour of optical conductivity $\sigma(\omega)$ in quasicrystals should be the summary effect of the same set of resonance absorption peaks.

The optical conductivity $\sigma(\omega)$ of $\text{Al}_{63}\text{Cu}_{25}\text{Fe}_{12}$ at room temperature is shown in Figure 7 in accordance with experimental data [39]. It presents an intense, broad and practically featureless (except for maximum) band occupying virtually the all range of frequencies from 40 up to $25,000 \text{ cm}^{-1}$. A number of authors have reported the existence of the similar bands in various icosahedral systems: AlPdMn [40], AlMnSi [41], AlPdRe [42], and AlCuFeB [43]. Accordingly, there exist three possible explanations for the band. It may be associated with strong scattering of electrons and then the maximum occurs at $\omega = 1/\tau$ [44]; it may be associated with the direct gap in the zone structure and

then $\sigma(\omega) = \text{const} \times (\omega - E_g)^{1/2} / \omega$ [42]; and, finally, it may be associated with resonance absorption [43] in the form of:

$$\sigma(\omega) \propto \sum_i \frac{\omega^2 \omega_i^2 \gamma_i}{(\omega_{0i}^2 - \omega^2)^2 + \omega^2 \gamma_i^2} \quad (8)$$

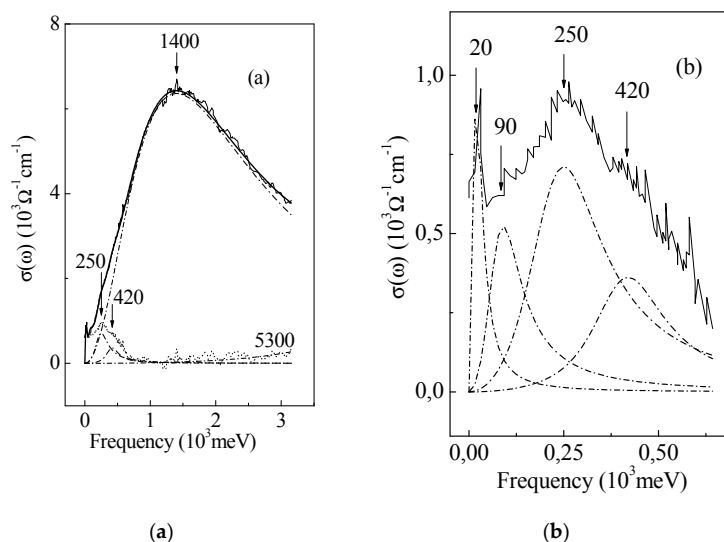


Figure 7. (a) Experimental optical conductivity of icosahedral $\text{Al}_{63}\text{Cu}_{25}\text{Fe}_{12}$ (thin solid line [39]). The dash-dotted line (1400) is a fit with the Lorentzian peak according to Equation (8). The dotted line is a residue after subtraction of the peak. Dash-dotted line (5300) is a fit with the Lorentzian peak according to Equation (8). Thick solid line is a fit with a sum of this Lorentzian peak and peaks in (b). (b) The residue shown in (a) but on an enlarged scale (solid line). Dash-dotted lines (20, 90, 250, and 420) are the fit with the Lorentzian peaks according to Equation (8).

Here, ω_{0i} , ω_i , and γ_i are the i th mode resonance frequency, damping, and mode strength of the i th harmonic oscillators, respectively.

In the latter case, the maximum occurs at $\omega_0 = \delta E_i$ directly. It was not so hard to see that the band maximum in $\text{Al}_{63}\text{Cu}_{25}\text{Fe}_{12}$ i -phase at about 1.4 eV coincides very well with $\delta E_i = 1400$ meV from tunnelling experiment. We used this coincidence to deconvolute the broad band for a set of elementary optic terms using a Lorentzian peak (Equation (8)) as a trial function.

First, we approximate the maximum as the best-defined feature with the reference at the upper part of the curve. The result is shown by dash-dotted line on Figure 7a. Intriguing was the difference between the experimental curve and the calculated curve "1400". This residual is shown in Figure 7a by dotted line and in Figure 7b at an enlarged scale by the solid line. Surprisingly, the visual revealed three peaks at about 420, 250 and 20 meV. There is a small residue in the high energy part of the spectrum. It is shown in Figure 7a by dotted line. The dash-dotted line shows the description of this residue by elementary term Equation (8) with $\delta E_i = 5300$ meV. Unfortunately, the maximum of the peak, if it exists, takes place outside the experimental range. As to the peak with the smallest excitation energy at about 5 meV in tunnelling experiment, it could not be observed at room temperature. To achieve the best description, shown by a thick solid line in Figure 7a, we needed yet another peak at 90 meV shown by dash-dotted line in Figure 7b.

Therefore, it can be considered that practically all the gaps identified in the tunnelling experiment were confirmed by an independent optical experiment.

6. TLEs and Giant Thermally Induced Effects in Magnetic Susceptibility and dc Conductivity

By analogy with the excess specific heat, it is reasonable to expect that the thermally induced components in conductivity and magnetic susceptibility can also be calculated by adding numerous elementary terms. Under this assumption, we analysed these components using the simplest supposition that $\sigma_t(T) = \sum \sigma_i$ and $\chi_t(T) = \sum \chi_i$, as well as that the elementary terms σ_i and χ_i are the linear functions of TLE density, i.e., $\sigma_i \propto N_{\text{TLE}i}$ (see Equation (3)) and $\chi_i \propto T^{-1} N_{\text{TLE}i}$. These terms were used as trial functions. The final results of this analysis are shown in Figures 8 and 9. An almost perfect curve fitting was achieved using the above-mentioned set of characteristic energies. It is surprising that such high-energy TLEs of up to 1400 meV were shown to be effective in a physical experiment.

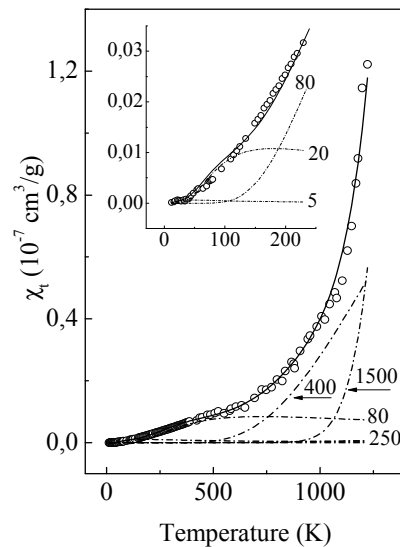


Figure 8. Temperature-dependent part of the magnetic susceptibility of the ordered $\text{Al}_{63}\text{Cu}_{25}\text{Fe}_{12}$ phase: (o), experimental results [2]; and solid line, description of the results by a sum of the magnetic elementary terms (dash-dotted lines) with $\delta E = 5, 16, 80, 260, 400,$ and 1500 meV, respectively.

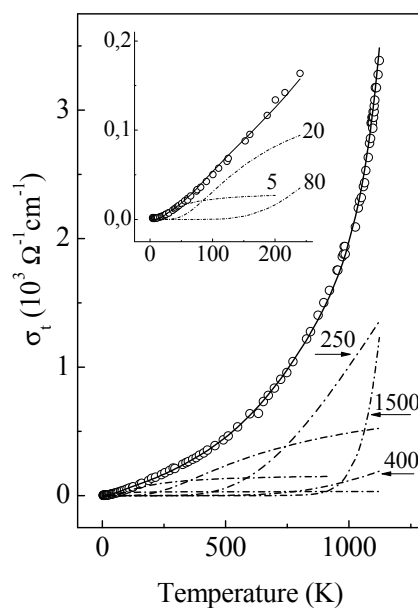


Figure 9. Temperature-dependent part of the dc conductivity of the ordered $\text{Al}_{63}\text{Cu}_{25}\text{Fe}_{12}$ phase: (o), experimental results [2]; and solid line, description of the results by a sum of the conduction elementary terms (dash-dotted lines) with $\delta E = 5, 16, 80, 260, 400,$ and 1500 meV, respectively.

As is well known, the Inverse Matthiessen Rule is difficult to understand from the classical thermally-activated mechanism point of view, since the temperature dependence of $\sigma(T)$ does not follow an exponential law having the form of $\exp(-E_g/k_B T)$ [45]. We argue that the reason for this is the multigap spectrum of threshold excitations.

7. Conclusions

Such, in general terms, are the implications of our supposition that an excess heat capacity in quasicrystals is electronic in nature and is a sum of the Schottky thermal anomalies. To complete the above, remains to update the model of the electronic structure proposed earlier [24,25], taking into account the new data. The most comprehensive spectrum of two-level excitations (seven terms) in the range of 5 to 5300 meV was achieved by analysis of the tunnel characteristics. A slightly narrower spectrum (six terms) from 20 to 5300 meV was produced by the analysis of the optical conductivity. Finally, excess heat capacity analysis revealed two types of excitations. It is remarkable that a variety of experimental tools have revealed, to a greater or lesser extent, the same row of characteristic energies. This evidences that this row is an essential feature of the systems discussed. For the Al-Cu-Fe i-phases studied, such a row is a set of characteristic energies 5, 19, 80, 250, 400, 1400 and 5300 meV. With this knowledge, the updated scheme of the two-component model of the electronic structure is presented in Figure 10.

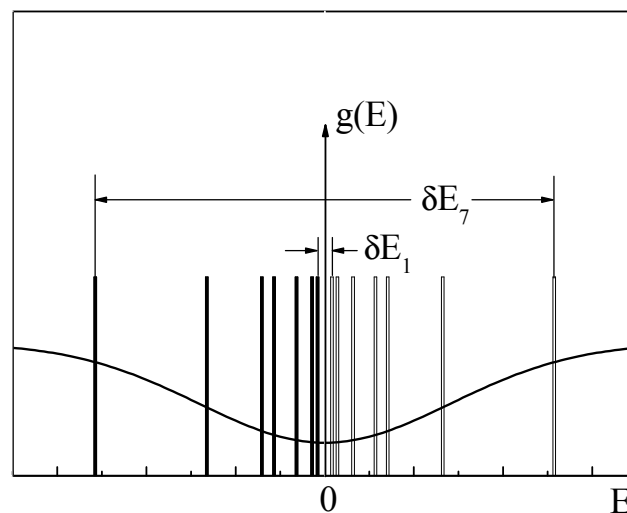


Figure 10. An updated version of the electronic structure model. Shown schematically is the superposition of two types of spectra: the continuum spectrum with a pseudogap and the discrete spectrum with seven types of two-level states. The Fermi level is fixed at the centre of the smallest gap separating the symmetric and antisymmetric states. For the sake of representativity, a nonlinear scale $E^{1/2}$ is used. To simplify, only the smallest (δE_1) and the largest (δE_7) gaps are indicated by arrows.

On the other hand, the supposition that the continual and discrete components in our model are autonomic subsystems is confirmed firmly enough by Ziner's mechanism of the fine structure of tunnel spectra.

Thus, the idea of designing the electronic structure with a simple (non-hybridizing) superimposition of continual and discrete components is confirmed by numerous experiments. Earlier, the idea was used in the theoretical model [46]. Discrete component has been included in the DOS model by means of a self-similar Dirac comb along with a parabolic pseudogap. There is impressive external similarity between Figure 10 and Figure 1 in [46]. The physical relevance of this similarity requires a further study.

To conclude, the purpose of this investigation was to see what new knowledge calorimetric experiments can provide to the solution of the problem of singular electronic states in quasicrystals.

Within the traditional understanding of the Schottky thermal anomalies, it can be definitely said that singular electronic states are a source of local two-level excitations and that the system of these excitations is not homogeneous. It should also be noted that with the present understanding of the nature of the residual metal-like carriers in quasicrystals, singular electronic states can coexist with the continuum of the conduction band states. The physicality of this implication also requires additional study.

Acknowledgments: We are grateful to Junpei Okada and Keiichi Edagawa for interest in the work. This work was supported by the Federal Agency of Scientific Organizations of the Russian Federation (Project No. 01201463333000, theme “Spin”) and in part by the Russian Foundation for Basic Research (Project No. 16-02-00085-a) and by the Complex Program of the Ural Branch, Russian Academy of Sciences (Project No. 15-17-2-12).

Author Contributions: Alexandre Prekul analysed data and wrote the paper; and Natalya Shchegolikhina analysed data and designed the article at whole.

Conflicts of Interest: The authors declare no conflict of interest.

References

1. Stadnik, Z.M.; Purdie, D.; Baer, Y.; Logarasso, T.A. Absence of fine structure in the photoemission spectrum of the icosahedral Al-Pd-Mn quasicrystal. *Phys. Rev. B* **2001**, *64*, 214202. [[CrossRef](#)]
2. Prekul, A.F.; Shchegolikhina, N.I. Correlations between Electric, Magnetic, and Galvanomagnetic Quantities in Stable Icosahedral Phases Based on Aluminum. *Crystallogr. Rep.* **2007**, *52*, 996–1005. [[CrossRef](#)]
3. Guo, Q.; Poon, S.J. Metal-insulator transition and localization in quasicrystalline $\text{Al}_{70.5}\text{Pd}_{21}\text{Re}_{8.5-x}\text{Mn}_x$ alloys. *Phys. Rev. B* **1996**, *54*, 12793. [[CrossRef](#)]
4. Janot, C.; de Boissieu, M. Quasicrystals as a hierarchy of clusters. *Phys. Rev. Lett.* **1994**, *72*, 1674. [[CrossRef](#)] [[PubMed](#)]
5. Janot, C. Atomic clusters, local isomorphism, and recurrently localized states in quasicrystals. *J. Phys. Condens. Matter.* **1997**, *9*, 1493. [[CrossRef](#)]
6. Gantmakher, V.F. Chemical localization. *Phys. Usp.* **2002**, *45*, 1165. [[CrossRef](#)]
7. Tsai, A.P.; Stadnik, Z.M. Physical Properties of Quasicrystals. In *Springer Series in Solid-State Science*; Springer: Berlin/Heidelberg, Germany, 1999; Volume 126, pp. 257–293.
8. Prekul, A.F.; Shchegolikhina, N.I.; Gaiduchenko, A.B.; Grushevskii, K.I. Comparative Study of the Heat Capacity of Icosahedral Quasicrystals in Solid and Liquid States. *Phys. Solid State* **2011**, *53*, 1987. [[CrossRef](#)]
9. Prekul, A.F.; Shchegolikhina, N.I.; Gaiduchenko, A.B.; Grushevskii, K.I. Electric, Magnetic, and Thermal Properties of Quasicrystal-Forming Melts. *JETP Lett.* **2011**, *94*, 366–369. [[CrossRef](#)]
10. Kirihara, K.; Nakata, T.; Takata, M.; Kubota, Y.; Nishibori, E.; Kimura, K.; Sakata, M. Covalent Bonds in AlMnSi Icosahedral Quasicrystalline Approximant. *Phys. Rev. Lett.* **2000**, *85*, 3468. [[CrossRef](#)] [[PubMed](#)]
11. Kirihara, K.; Nagata, T.; Kimura, K.; Kato, K.; Takata, M.; Nishibori, E.; Sakata, M. Covalent bonds and their crucial effects on pseudogap formation in $\alpha\text{-Al}(\text{Mn},\text{Re})\text{Si}$ icosahedral quasicrystalline approximant. *Phys. Rev. B* **2003**, *68*, 014205. [[CrossRef](#)]
12. Kirihara, K.; Kimura, K. Sign of covalency in AlPdRe icosahedral quasicrystals obtained from atomic density and quasilattice constant. *Phys. Rev. B* **2001**, *64*, 212201. [[CrossRef](#)]
13. Born, M. *Atomic Physics*; Chapter 9; Blackie & Son Ltd.: London, UK, 1963.
14. Walti, Ch.; Felder, E.; Chernikov, M.A.; Ott, H.R.; de Boissieu, M.; Janot, C. Lattice excitations in icosahedral Al-Mn-Pd and Al-Re-Pd. *Phys. Rev. B* **1998**, *57*, 504. [[CrossRef](#)]
15. Chernikov, M.A.; Bernasconi, A.; Beeli, C.; Schilling, A.; Ott, H.R. Low-temperature magnetism in icosahedral $\text{Al}_{70}\text{Mn}_9\text{Pd}_{21}$. *Phys. Rev. B* **1993**, *48*, 3058. [[CrossRef](#)]
16. Lasjaunias, J.C.; Calvayrac, Y.; Yang, H. Investigation of Elementary Excitations in AlCuFe Quasicrystals by Means of Low-Temperature Specific Heat. *J. Phys. I Fr.* **1997**, *7*, 959–976. [[CrossRef](#)]
17. Inaba, A.; Takakura, H.; Tsai, A.P.; Fisher, I.R.; Canfield, P.C. Heat capacities of icosahedral and hexagonal phases of Zn-Mg-Y system. *Mater. Sci. Eng.* **2000**, *294–296*, 723–726. [[CrossRef](#)]
18. Prekul, A.F.; Kazantsev, V.A.; Shchegolikhina, N.I.; Gulyaeva, R.I.; Edagawa, K. High-Temperature Heat Capacity of the $\text{Al}_{63}\text{Cu}_{25}\text{Fe}_{12}$ Quasicrystal. *Phys. Solid State* **2008**, *50*, 2013–2015. [[CrossRef](#)]
19. Charles, K. *Introduction to Solid State Physics*; Chapter 6; John Wiley and Sons, Inc.: New York, NY, USA, 1956.

20. Prekul, A.F.; Shchegolikhina, N.I.; Podgornykh, S.M. Gruneisen's law and particularities of electronic excitations in quasicrystals. *Low Temp. Phys.* **2009**, *35*, 536. [[CrossRef](#)]
21. Prekul, A.F.; Shalaeva, E.V.; Shchegolikhina, N.I. Calorimetric Investigation of Electronic and Lattice Excitations of the Icosahedral Quasicrystal in the Range of Moderate Temperatures. *Phys. Solid State* **2010**, *52*, 1797. [[CrossRef](#)]
22. Prekul, A.F.; Shchegolikhina, N.I.; Edagawa, K. On nature of the excess heat capacity in the icosahedral quasicrystals. *Philos. Mag.* **2011**, *91*, 2828. [[CrossRef](#)]
23. Keesom, W.H.; Pearlman, N. *Handbook der Physik*; Springer: Verlag, Berlin, Germany, 1956.
24. Prekul, A.F.; Shchegolikhina, N.I.; Shalaeva, E.V. Inhomogeneous Electronic Localization in Icosahedral Quasicrystals. *Acta Phys. Polon. A* **2014**, *126*, 556–559. [[CrossRef](#)]
25. Prekul, A.F.; Shchegolikhina, N.I. Short-Range Order and Singularities of the Electronic Structure of Icosahedral Quasicrystals. *Phys. Solid State* **2013**, *55*, 2260–2266. [[CrossRef](#)]
26. Klein, T.; Berger, C.; Mayou, D.; Cyrot-Lackmann, F. Proximity of a Metal-Insulator Transition in Icosahedral Phases of High Structural Quality. *Phys. Rev. Lett.* **1991**, *66*, 2907. [[CrossRef](#)] [[PubMed](#)]
27. Mott, N.F.; Davis, E.A. *Electronic Processes in Noncrystalline Materials*; Chapter 2; Clarendon Press: Oxford, UK, 1971.
28. Escudero, R.; Lasjaunias, J.C.; Calvayrac, Y.; Boudard, M. Tunnelling and point contact spectroscopy of the density of states in quasicrystalline alloys. *J. Phys. Condens. Matter* **1999**, *11*, 383. [[CrossRef](#)]
29. Li, G.H.; He, H.F.; Wang, Y.P.; Lu, L.; Li, S.L.; Jing, X.N.; Zhang, D.L. Tunneling spectroscopy in AlNiCo decagonal quasicrystals. *Phys. Rev. Lett.* **1999**, *82*, 1229.
30. Klein, T.; Symko, O.G.; Davydov, D.N.; Jansen, A.M. Observation of a narrow pseudogap near the Fermi level of AlCuFe quasicrystalline thin films. *Phys. Rev. Lett.* **1995**, *74*, 3656. [[CrossRef](#)] [[PubMed](#)]
31. Davydov, D.N.; Mayou, D.; Berger, C.; Gignoux, C.; Neumann, A.; Janssen, A.G.M.; Wyder, P. Density of states in quasicrystals and approximants: Tunneling experiment on bare and oxidized surfaces. *Phys. Rev. Lett.* **1996**, *77*, 3173. [[CrossRef](#)] [[PubMed](#)]
32. Okada, J.T.; Ekino, T.; Yokoyamas, Y.; Takasaki, T.; Watanabe, Y.; Nanao, S. Evidence of the fine pseudogap at the Fermi level in Al-based quasicrystals. *J. Phys. Soc. Jpn.* **2007**, *76*, 033707. [[CrossRef](#)]
33. Widmer, R.; Groning, O.; Ruffieux, P.; Groning, P. Low-temperature scanning tunneling spectroscopy on the 5-fold surface of the icosahedral AlPdMn quasicrystals. *Philos. Mag.* **2006**, *86*, 781–787. [[CrossRef](#)]
34. Mader, R.; Widmer, R.; Groning, P.; Ruffieux, P.; Steurer, W.; Groning, O. A comparative scanning tunneling spectroscopy investigation of the (12110)-surface of decagonal Al–Ni–Co and the (100)-surface of its approximant Y–Al–Ni–Co. *New J. Phys.* **2010**, *12*, 073043. [[CrossRef](#)]
35. Mader, R.; Widmer, R.; Groning, P.; Steurer, W.; Groning, O. Correlating scanning tunneling spectroscopy with the electrical resistivity of Al-based quasicrystals and approximants. *Phys. Rev. B* **2013**, *87*, 075425. [[CrossRef](#)]
36. Delahaye, J.; Schaub, T.; Berger, C. Tunneling spectroscopy and high electrical resistivity in quasicrystalline alloys. *Philos. Mag.* **2006**, *86*, 789–796. [[CrossRef](#)]
37. Chynoweth, A.G. Internal Field Emission. *Prog. Semicond.* **1960**, *4*, 95.
38. Prekul, A.F.; Shchegolikhina, N.I. Internal Field Emission Nature of the Fine Structure of Tunnel Spectra in Icosahedral Quasicrystals. *JETP Lett.* **2016**, *103*, 603–606. [[CrossRef](#)]
39. Homes, C.C.; Timusk, T.; Wu, X. Optical conductivity of the stable icosahedral Al_{63.5}Cu_{24.5}Fe₁₂. *Phys. Rev. Lett.* **1991**, *67*, 2694. [[CrossRef](#)] [[PubMed](#)]
40. Degiorgi, L.; Chernikov, M.A.; Beeli, C.; Ott, H.R. The electrodynamic response of the icosahedral quasicrystals Al₇₀Mn₉Pd₂₁. *Solid State Commun.* **1993**, *87*, 721–726. [[CrossRef](#)]
41. Wu, X.; Homes, C.C.; Burkov, S.E.; Timusk, T.; Pierce, F.C.; Poon, S.J.; Cooper, S.L.; Karlov, M.A. Optical conductivity of the icosahedral quasicrystals Al_{75.5}Mn_{20.5}Si₄ and its 1/1 crystalline approximant α -Al_{72.5}Mn_{17.4}Si_{10.1}. *J. Phys. Condens. Matter.* **1993**, *5*, 5975–5990. [[CrossRef](#)]
42. Basov, D.N.; Pierce, F.S.; Volkov, P.; Poon, S.J.; Timusk, T. Optical conductivity of insulating Al-based alloys: Comparison of quasiperiodic and periodic systems. *Phys. Rev. Lett.* **1994**, *73*, 1865–1868. [[CrossRef](#)] [[PubMed](#)]
43. Demange, V.; Milandri, A.; de Weerd, M.C.; Machizaud, F.; Jeandel, G.; Dubois, J.M. Optical conductivity of Al–Cr–Fe approximant compounds. *Phys. Rev. B* **2002**, *65*, 144205. [[CrossRef](#)]

44. Burkov, S.E.; Timusk, T.; Ashcroft, N.W. Optical conductivity of icosahedral quasi-crystals. *J. Phys. Condens. Matter.* **1992**, *4*, 9447–9458. [[CrossRef](#)]
45. Macia, E. Universal features in the electrical conductivity of icosahedral Al-transition-metal quasicrystals. *Phys. Rev. B* **2002**, *66*, 174203. [[CrossRef](#)]
46. Macia, E. Modeling the electric conductivity of icosahedral quasicrystals. *Phys. Rev. B* **2000**, *66*, 8771.



© 2016 by the authors; licensee MDPI, Basel, Switzerland. This article is an open access article distributed under the terms and conditions of the Creative Commons Attribution (CC-BY) license (<http://creativecommons.org/licenses/by/4.0/>).